telecom

MDPI

Article

Joint Placement Optimization and Sum Rate Maximization of RIS-Assisted UAV with LEO-Terrestrial Dual Wireless Backhaul

Naba Raj Khatiwoda, Babu R. Dawadi * and Shashidhar R. Joshi

Department of Electronics and Computer Engineering, Pulchowk Campus, Institute of Engineering, Tribhuvan University, Kathmandu 19753, Nepal; ernabaraj@gmail.com (N.R.K.); srjoshi@ioe.edu.np (S.R.J.)
* Correspondence: baburd@ioe.edu.np

Abstract

Achieving ubiquitous coverage in 6G networks presents significant challenges due to the limitations of high-frequency signals and the need for extensive infrastructure, and providing seamless connectivity in remote and rural areas remains a challenge. We propose an integrated optimization framework for UAV-LEO-RIS-assisted wireless networks, aiming to maximize system sum rate through the strategic placement and configuration of Unmanned Aerial Vehicles (UAVs), Low Earth Orbit (LEO) satellites, and Reconfigurable Intelligent Surfaces (RIS). The framework employs a dual wireless backhaul and utilizes a grid search method for UAV placement optimization, ensuring a comprehensive evaluation of potential positions to enhance coverage and data throughput. Simulated Annealing (SA) is utilized for RIS placement optimization, effectively navigating the solution space to identify configurations that improve signal reflection and network performance. For sum rate maximization, we incorporate several metaheuristic algorithms, including Particle Swarm Optimization (PSO), Genetic Algorithm (GA), Grey Wolf Optimization (GWO), Salp Swarm Algorithm (SSA), Marine Predators Algorithm (MPA), and a hybrid PSO-GWO approach. Simulation results demonstrate that the hybrid PSO-GWO algorithm outperforms individual metaheuristics in terms of convergence speed and achieving a higher sum rate. The coverage improves from 62% to 100%, and the results show an increase in spectrum efficiency of 23.7%.

Keywords: UAV; RIS; LEO; placement optimization; NTN networks; phase shift optimization; sum rate

Academic Editors: Sarun Duangsuwan and George Tsoulos

Received: 31 May 2025
Revised: 7 July 2025
Accepted: 6 August 2025
Published: 18 August 2025

Citation: Khatiwoda, N.R.; Dawadi, B.R.; Joshi, S.R. Joint Placement Optimization and Sum Rate Maximization of RIS-Assisted UAV with LEO-Terrestrial Dual Wireless Backhaul. *Telecom* **2025**, *6*, 61. https://doi.org/10.3390/telecom6030061

1. Introduction

In the Beyond 5G (B5G) and 6G wireless communication landscape, it becomes critical to ensure ubiquitous and reliable coverage, especially in challenging or underserved environments such as rural areas, urban canyons, disaster zones, and dense urban networks [1,2], although we can optimize the coverage and capacity of 5G using existing 4G infrastructure [3]. The unmanned aerial vehicle—reconfigurable intelligent surfaces (UAV-RIS) technology provides a solution to these challenges by dynamically expanding and enhancing wireless coverage. UAVs provide flexible on-demand deployment that rapidly adapts to user distribution and network conditions, while RIS enables energy-efficient beamforming [4] and channel reconfiguration without active transmission. The synergy between UAVs and RIS facilitates intelligent and cost-effective wireless coverage by overcoming obstacles, mitigating signal blockages, and optimizing spectral efficiency in 3D space. This becomes especially relevant for 6G goals such as 3D global coverage,

extreme data rates, and intelligent networking. By integrating UAV-RIS systems, networks can achieve higher connectivity reliability, improved coverage continuity, and green communication objectives, positioning this technology as a cornerstone in the realization of robust, adaptive, and future-proof wireless infrastructures [5].

Low earth orbit (LEO) UAV-RIS networks represent an emerging paradigm for B5G and 6G communication systems, combining the global coverage of LEO satellite constellations with the flexible deployment of UAVs augmented by RIS to form a space–air–ground integrated architecture [6,7]. LEO satellites offer reduced latency and ubiquitous three-dimensional coverage critical for real-time, mission-critical applications [8]. UAVs equipped with RIS can dynamically adjust their positions and surface configurations to reconstruct reliable air-to-ground links, mitigate blockages, and steer beams toward ground users, significantly enhancing link quality and spectrum efficiency [9]. RIS modules exploit passive reflection elements to achieve cost- and energy-efficient beam management, reducing Doppler shift effects and inter-beam interference in satellite links. In B5G contexts, these networks support high-throughput, low-latency IoT and edge services, while in 6G scenarios, they underpin advanced use cases such as holographic communications, digital twins, and autonomous systems by enabling intelligent, adaptive electromagnetic environments [10]. Furthermore, the integration of LEO, UAV, and RIS aligns with 3GPP non-terrestrial network standardization efforts, promising scalable and resilient connectivity for remote and underserved regions with minimal infrastructure investment [11]. Recent research also explores resource allocation and UAV trajectory optimization to further maximize spectral efficiency in these hybrid networks [12].

Dual backhaul systems for UAV-RIS networks combine a satellite link and a terrestrial link to provide robust, high-availability connectivity and mitigate failures in extreme conditions. This hybrid architecture enables UAV-mounted RIS panels to dynamically optimize both channels through passive beam steering and link selection algorithms, balancing the satellite link's path diversity with the terrestrial link's capacity to enhance spectral efficiency and reliability for B5G/6G NTN applications [13,14].

In UAV-RIS networks, coverage optimization entails strategically positioning UAVs and orienting RIS panels to mitigate blockages and maximize ground-to-user coverage, often formulated as mixed-integer nonlinear programs to ensure full area illumination and user connectivity [15]. Phase shift optimization focuses on designing optimal reflection coefficients for RIS elements using convex approximation or alternating optimization methods to steer electromagnetic waves toward intended receivers, enhancing received power and counteracting path loss [16]. Sum rate optimization jointly tunes UAV trajectories, power allocation, and RIS phase configurations to maximize total network throughput under QoS constraints, typically leveraging successive convex approximation or iterative block coordinate descent algorithms [17]. By integrating coverage, phase shift, and sum rate optimization frameworks, UAV-RIS systems deliver robust, high capacity links for B5G/6G non-terrestrial networks (NTN), enabling seamless connectivity in complex environments [18]. The major contributions of this study are as follows:

- We propose a novel dual wireless backhaul system for RIS-assisted UAV and LEO networks for reliable communications.
- We formulate an UAV placement optimization using a grid search algorithm for better line of site (LOS) between the UAV and Users.
- We optimize the placement of RIS with optimized UAV using the Simulated Annealing (SA) algorithm to connect all the users for reliable communications.
- We maximize the sum rate through phase shift optimization using metaheuristic algorithms: PSO, GWO, SSA, MPA, GA, and hybrid PSO-GWO.

The remainder of the paper is organized as follows: Section 2 presents background and related works carried out for NTN networks. Section 3 outlines the procedure and methodologies, the problem formulation procedure that we adopted, and the algorithms used to solve these problems. Section 4 presents the output and results that we calculate, and the improvement of the results using the algorithms. Finally, Section 5 concludes the paper with recommendations for future works.

2. Related Work

Recent literature has extensively explored UAV-mounted RIS placement strategies to enhance ground coverage in terrestrial environments, employing mixed-integer nonlinear programming and metaheuristic algorithms to determine optimal UAV altitudes and horizontal coordinates for RIS deployment [19,20]. Coverage optimization studies model urban blockage scenarios by integrating UAV-mounted RIS panels to dynamically steer mmWave beams, demonstrating significant improvements in coverage ratio over conventional UAV-only systems through joint three-dimensional placement and orientation algorithms [21].

Phase shift optimization research has focused on designing optimal reflection coefficients for RIS elements via alternating optimization and convex relaxation techniques, significantly boosting received signal power and mitigating path loss. Sum rate maximization frameworks jointly tune UAV trajectories, transmit power, and RIS phase configurations, often leveraging successive convex approximation or block coordinate descent methods, achieving notable throughput gains in multi-user downlink scenarios [22–25].

Extensions to non-terrestrial networks integrate LEO satellite backhauls with UAV-RIS nodes, where aerial-RIS panels assist satellite beams to extend coverage and throughput while optimizing aerial placement and phase design under backhaul constraints [26]. These related works underscore the critical interplay between UAV-RIS placement, coverage, and phase shift optimization in advancing both terrestrial and non-terrestrial B5G/6G network architectures.

In obstacle-oriented environments, UAV-mounted RIS placement must jointly consider three-dimensional line-of-sight (LoS) blockage models derived from high resolution obstacle maps to ensure reliable connectivity, with path planning algorithms adapting UAV positions in real time to avoid blockages and maintain coverage quality. Recent formulations treat the placement problem as a non-convex, NP-hard optimization, where metaheuristic methods are used to optimize UAV location and RIS orientation to maximize sum rate under Rician fading channels [27,28].

Blockage awareness is enhanced by integrating ray tracing or statistical blockage models into the objective, enabling adaptive phase shift optimization of RIS elements to steer beams around obstacles and boost received power, which has been shown to yield significant throughput gains in urban scenarios [29].

Simulation studies in both dense urban and indoor testbeds demonstrate that obstacle-aware UAV-RIS frameworks can improve sum rate significantly over baseline UAV-only deployments, by dynamically repositioning aerial-RIS nodes and reconfiguring phase shifts in response to user mobility and obstacle dynamics [30]. The literature lacks reliability and uniform coverage, and we are motivated to address the problems by proposing a dual wireless backhaul system for NTN networks in the B5G and 6G networks for reliable communication and ubiquitous connectivity.

3. System Model and the Problem Formulations

We consider a RIS-assisted UAV communication network utilizing a dual wireless backhaul, comprising one Ground Earth Station (GES) to LEO to UAV (GES-LEO-UAV)

and another BTS-UAV link, operating in both active and standby modes at a frequency of 28 GHz. Dual wireless backhaul is vital for reliable network operation, even if one of the links fails. Figure 1 shows a schematic diagram for RIS-assisted UAV networks with a dual wireless backhaul system in a blockage scenario where the UAV is placed in the center of 2D grids initially at a height of 50 m and then optimized the positions using a grid search algorithm to improve the LOS users. The UAV-Users networks in the proposed RIS-assisted UAV networks act as an access network and communicate with users directly at LOS. UAV-RIS-user networks are used to provide access to NLOS users by deploying the necessary RISs using SA to make all users LOS. Dual wireless backhaul networks provide connectivity between the core networks and the access networks, ensuring reliable operations. Phase shift optimization is carried out using metaheuristic algorithms to maximize the sum rate.

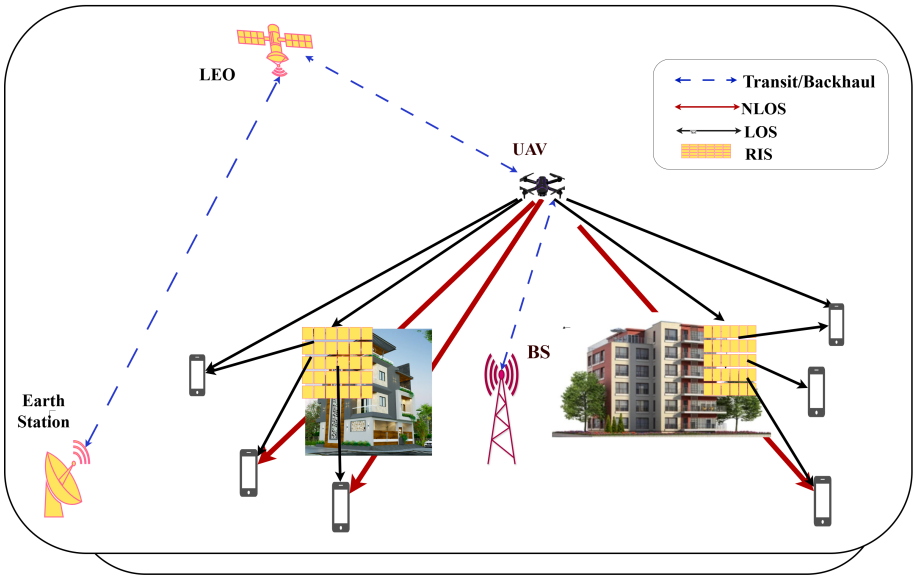

Figure 1. An RIS-assisted UAV communication network with dual wireless backhaul.

3.1. Backhaul Link Budget

3.1.1. Link Budget Calculation for BS-to-UAV at 28 GHz

To assess the signal strength from a ground-based Base Station (BS) to a UAV operating at millimeter wave frequencies, particularly at 28 GHz, a link budget analysis is performed using the Friis transmission equation under free space Line of Sight (LOS) conditions. The received power at the UAV is given by Equation (1),

$$P_r(\text{UAV}) = P_t + G_t + G_r - L_p - L_m \quad [\text{dBm}] \tag{1}$$

where P_t is the BS transmit power (dBm), G_t and G_r are the transmitter and receiver antenna gains (dBi), L_p is the free space path loss (dB), and L_m accounts for miscellaneous system losses such as cable attenuation and fading margin. The free-space path loss (FSPL) is given as $\left(\frac{4\pi d}{\lambda}\right)^2$ and computed in dBm using Equation (2),

$$L_p = 20\log_{10}(d) + 20\log_{10}(f) - 147.55 \quad [\text{dBm}] \tag{2}$$

where d is the distance in meters and f is the carrier frequency in Hz. The significant propagation loss in the mmWave band, even over relatively short distances, draws attention to designing a system with high gain antennas, optimized UAV positioning, or using RIS to maintain reliable connectivity. Recent works have investigated similar mmWave

aerial link scenarios, offering insights into link optimization and advanced enhancement techniques [31–34].

3.1.2. Bachhaul Networks and Link Budget

The link budget for a communication link between a ground-based Earth station and a LEO satellite quantitatively determines the received signal power and the overall quality of the communication link. The procedure begins by computing the Free Space Path Loss (FSPL) using Equation (2). The Effective Isotropic Radiated Power (EIRP) is calculated as Equation (3),

$$\text{EIRP} = P_t + G_t - L_{\text{tx}} \quad [\text{dBm}] \tag{3}$$

where P_t is the transmit power (in dBm), G_t is the transmitter antenna gain (dBi), and L_{tx} accounts for transmitter-side losses. The received power at the LEO is given by Equation (4),

$$P_r = \text{EIRP} + G_r - L_{\text{FSPL}} - L_{\text{rx}} - L_{\text{atm}} \quad [\text{dBm}] \tag{4}$$

where G_r is the receiver antenna gain, L_{rx} includes receiver-side losses, and L_{atm} models atmospheric attenuation, especially significant at Ka-band frequencies such as 28 GHz. The thermal noise power at the receiver is computed as in Equation (5),

$$N = 10\log_{10}(kTB) + 30 + NF \quad [\text{dBm}] \tag{5}$$

where k is the Boltzmann constant (1.38×10^{-23} J/K), T is the system noise temperature (K), B is the receiver bandwidth (Hz), and NF is the receiver noise figure (dB). The Carrier-to-Noise Ratio (C/N) is then given by Equation (6),

$$\frac{C}{N} = P_r - N \quad [\text{dB}] \tag{6}$$

This metric is a key indicator of link quality and is used to assess whether the communication system can meet the required modulation and coding thresholds. This analytical approach forms the backbone of satellite communication performance evaluations and can be extended to more complex models, including Rician fading and link margin analysis [35–38].

3.2. Access Networks

The access networks comprise UAVs, RISs, and users. Networks face different environmental challenges, such as rain, thunderstorms, and infrastructure constraints, such as buildings and trees, which degrade the strength of the signal and affect the QOS of the system. A UAV is deployed as an aerial base station in the considered simulation topology to provide wireless coverage in an urban-like environment. The deployment area is a square region of size 300 m × 300 m, within which the UAV is positioned exactly at the geometric center, i.e., at coordinates (150 m, 150 m), and maintained at a fixed altitude of 100 m above ground level. This central aerial deployment ensures symmetrical coverage potential across the area. A set of ground users is randomly distributed within the x-y plane at ground level using a uniform spatial distribution, representing a realistic and unstructured user layout.

Next, the geometric environment is laid out by randomly dropping ground users across a rectangle $[x_{\min}, x_{\max}] \times [y_{\min}, y_{\max}]$, each at height h_u. Buildings are specified as footprints$\{(x,y)\colon x_{\min} \le x \le x_{\max},\ y_{\min} \le y \le y_{\max}\}$ extruded to height h_b. Any user whose (x,y) coordinate satisfies $\{x_{\min} \le x \le x_{\max},\ y_{\min} \le y \le y_{\max}\}$ for any building is removed, since they would lie inside that structure. The heart of the LOS blockage test casts a ray from the UAV at $(x_{\text{UAV}},\ y_{\text{UAV}},\ h_{\text{UAV}})$ down to each user at $(x_u,\ y_u,\ h_u)$. If the

projection of this ray intersects a building's footprint at $(x_{\text{int}},\ y_{\text{int}})$, we compute the ray's altitude there by linear interpolation using Equation (7),

$$h_{\text{ray}} = h_{\text{UAV}} + (h_u - h_{\text{UAV}})\,\frac{d_{\text{int}}}{d_{\text{tot}}} \tag{7}$$

where

$$d_{\text{int}} = \sqrt{(x_{\text{int}} - x_{\text{UAV}})^2 + (y_{\text{int}} - y_{\text{UAV}})^2}, \quad d_{\text{tot}} = \sqrt{(x_u - x_{\text{UAV}})^2 + (y_u - y_{\text{UAV}})^2}$$

If $h_{\text{ray}} \leq h_b$, the link is blocked.

To address non-line-of-sight (NLOS) challenges arising due to urban obstacles, RISs are strategically mounted on building walls. These RIS units are placed at optimized locations and elevations to reflect and steer the UAV's signal toward blocked users, effectively restoring LOS connectivity. The obstacles in the environment are modeled as rectangular prisms (cuboids), each representing a building or large urban structure. These obstacles are defined by their base coordinates in the x-y plane and are assigned a fixed height of 50 m. The presence of these obstacles introduces realistic shadowing effects and necessitates LOS checking using ray casting or geometric intersection methods between the UAV, RIS, and users [39]. The UAV alone initially attempts to cover as many users as possible, after which RISs are incrementally deployed on visible building surfaces to assist NLOS users until full coverage is achieved. In the proposed framework, a UAV-enabled communication system is designed to maximize ground user coverage by ensuring LOS connectivity through both direct UAV-user links and RIS-assisted reflections. The UAV is initially placed at a fixed altitude, and a grid search algorithm is applied over a predefined 3D grid to find the optimal UAV position that covers the maximum number of users with LOS [40,41]. Algorithm 1 illustrates the detailed procedure for grid search.

Algorithm 1 Grid Search for Optimal UAV Coverage

Input: Search bounds $areaXlim$, $areaYlim$, user positions $userPos$, heights $userHeight$, UAV height $uavHeight$, buildings bx, by, bh
Output: Optimal UAV position $uavPos$, coverage percentage $covPct$
Initialize grid: $xGrid$, $yGrid$ with step size $gridStep$
Initialize: $coverMat \leftarrow 0$, $coverageList \leftarrow 0$, $bestCover \leftarrow -\infty$
for each $x_i \in xGrid$ **do**
    for each $y_i \in yGrid$ **do**
        Initialize $blocked[k] \leftarrow$ false, $\forall k$
        for each user k **do**
            for each building j **do**
                Check intersection (x_{int}, y_{int}) between UAV-user line and building j
                if intersection exists **then**
                    Compute d_{int} and d_{tot} (distance to user and to intersection)
                    Compute intersection height (Equation (7))
                    if $rayH \leq bh[j]$ **then**
                        $blocked[k] \leftarrow$ true; **break**
                    end if
                end if
            end for
        end for
        Compute coverage: cf (Equation (10))
        Update $coverMat(y_i, x_i)$ and $coverageList$
        if $cf > bestCover$ **then**
            $bestCover \leftarrow cf$, $bestPos \leftarrow (x_i, y_i)$
        end if
    end for
end for
$uavPos \leftarrow bestPos$, $covPct \leftarrow bestCover \times 100$

3.2.1. UAV Placement Optimization with LOS Constraints

In this work, a blockage-aware grid search strategy is adopted to determine the optimal two-dimensional placement of a UAV flying at a fixed altitude, aimed at maximizing the coverage of ground users in an environment with building obstructions. The UAV is assumed to operate at a constant height, and its horizontal coordinates (x, y) are varied over a discrete grid $\mathcal{G} \subset \mathbb{R}^2$. For each candidate location, the algorithm evaluates whether a LOS connection exists between the UAV and each user by performing geometric intersection checks against 3D building models. A user is considered covered only if the direct signal path is unobstructed or if the height of the signal ray at the point of intersection is greater than the height of the obstructing building. The optimization objective is to maximize the ratio of users who have LOS connectivity to the UAV. Mathematically, the problem is formulated as shown in Equation (8):

$$\max_{(x,y)\in\mathcal{G}} \quad \frac{1}{N_u} \sum_{k=1}^{N_u} \mathrm{LOS}_k(x, y), \tag{8}$$

subject to the constraint in Equation (9):

$$(x, y) \in \mathcal{G}, \quad \text{and} \quad \mathrm{LOS}_k(x, y) \in \{0, 1\}, \quad \forall k. \tag{9}$$

where N_u is the total number of ground users, and $\mathrm{LOS}_k(x, y)$ is a binary function that returns 1 if user k has unobstructed LOS to the UAV at position (x, y), and 0 otherwise. This formulation ensures that UAV placement is environmentally aware, accounting for urban obstructions and terrain features. Such blockage-sensitive modeling has been emphasized in recent studies that integrate realistic 3D map data and spatial visibility constraints into UAV deployment and trajectory design. Moreover, this grid search strategy provides a performance baseline for more advanced optimization approaches, such as RIS-assisted or learning-based UAV placement frameworks [42–45]. The LOS condition for each user is evaluated through geometric visibility checks, and the overall coverage is calculated as shown in Equation (10).

$$\text{Coverage} = \frac{\text{Number of users with LOS}}{\text{Total number of users}} \times 100\% \tag{10}$$

If some users remain uncovered due to urban blockages, RISs are strategically added on building walls one by one, starting with a single RIS until all of the users are in LOS either with a UAV or any one of the RISs. RIS placement is optimized using SA.

3.2.2. RIS Placement Optimization Using SA

In the context of RIS-assisted wireless communication, optimal placement of RIS is a crucial factor influencing overall coverage, signal strength, and energy efficiency. The RIS placement problem is inherently non-convex and combinatorial, particularly in dynamic environments involving obstacles, user mobility, and multiple constraints such as LOS conditions.

SA, a stochastic optimization algorithm inspired by the physical annealing process, is well suited to handle such complex scenarios due to its ability to escape local optima and efficiently explore high-dimensional search spaces. Unlike gradient-based methods that may get trapped in suboptimal solutions, SA probabilistically accepts worse solutions at higher temperatures, enabling it to traverse rugged objective landscapes effectively. This makes SA particularly advantageous in RIS placement tasks where both discrete (e.g., candidate building positions) and continuous (e.g., height or tilt angles) variables must be jointly optimized. Furthermore, its simplicity and low computational overhead make it attractive for

real-time or adaptive placement schemes in RIS models supported by UAV or LEO. Overall, the integration of SA into the RIS placement model offers a robust and flexible solution strategy to improve system performance under practical deployment conditions [46–48].

We aim to maximize the coverage of users not already served by a UAV by optimally placing a fixed number of RIS units on candidate building wall positions. Let N_u be the number of users, $\mathcal{C} = \{\mathbf{c}_1, \ldots, \mathbf{c}_{N_c}\}$ the set of candidate RIS positions, and $\mathcal{B}$ the set of all buildings. The RIS placement decision set is $\mathcal{S} = \{\mathbf{r}_1, \ldots, \mathbf{r}_{N_{\text{RIS}}}\} \subseteq \mathcal{C}$, where N_{RIS} is fixed. The optimization problem is formulated in Equation (11).

$$\max_{\mathcal{S} \subset \mathcal{C}, |\mathcal{S}| = N_{\text{RIS}}} \quad \frac{1}{N_u} \sum_{k=1}^{N_u} \text{mask}_k \tag{11}$$

where $\text{mask}_k \in \{0, 1\}$ indicates whether user k is covered either directly or via RIS. The coverage condition for each user is defined as in Equation (12):

$$\text{mask}_k = \begin{cases} 1, & \text{if LOS}(\mathbf{u}, \mathbf{u}_k, \mathcal{B}) = 1 \\ 1, & \text{if } \exists\, \mathbf{r}_j \in \mathcal{S} \text{ s.t. LOS}(\mathbf{u}, \mathbf{r}_j, \mathcal{B} \setminus \mathcal{B}_{r_j}) = 1 \\ & \quad \text{and LOS}(\mathbf{r}_j, \mathbf{u}_k, \mathcal{B} \setminus \mathcal{B}_{r_j}) = 1 \\ 0, & \text{otherwise} \end{cases} \tag{12}$$

where $\mathcal{B}_{r_j}$ denotes the building to which RIS j is mounted, excluded from LOS checks to allow reflections. Algorithm 2 outlines the detailed procedure for SA optimization in RIS placement. The minimization of the number of RIS deployments after UAV placement optimization is formulated as in Equation (13),

$$\min_{\mathbf{x}_{\text{RIS}}} \left(\sum_{i=1}^{N_u} 1_{\text{uncovered}}(i) \right) \tag{13}$$

where $\mathbf{x}_{\text{RIS}}$ denotes the candidate RIS positions and N_u is the total number of users.

3.2.3. Rician Channel Model for UAV–RIS–User Communication

In UAV-assisted wireless networks enhanced by RIS, the communication links are often dominated by strong LOS components, particularly at millimeter wave frequencies. As such, the Rician fading model is especially suitable for modeling small scale fading in UAV-RIS-user systems, capturing both deterministic LOS and scattered NLOS effects. The Rician fading coefficient is given by Equation (14),

$$h = \sqrt{\frac{K}{K+1}} h_{\text{LOS}} + \sqrt{\frac{1}{K+1}} h_{\text{NLOS}} \tag{14}$$

where h_{LOS} is the LOS component, $h_{\text{NLOS}} \sim \mathcal{CN}(0, 1)$ models the scattered NLOS paths, and K is the Rician K factor representing the power ratio between LOS and NLOS components.

In a RIS-assisted UAV communication link, the effective end-to-end channel is expressed as in Equation (15),

$$h_{\text{eff}} = h_{BU} + \sum_{n=1}^{N} h_{RU}^{(n)} \theta_n h_{BR}^{(n)}, \tag{15}$$

where h_{BU} denotes the direct UAV-user link, $h_{BR}^{(n)}$ and $h_{RU}^{(n)}$ are the channels from the UAV to the n-th RIS element and from the RIS to the user, respectively, and $\theta_n = e^{j\phi_n}$ represents the adjustable phase shift applied by the n-th RIS element.

The received signal-to-noise ratio (SNR) at the user is given by Equation (16),

$$\gamma = \frac{P_t G_t G_r |h_{\text{eff}}|^2}{L_{\text{path}} N_0}, \quad \text{with} \quad L_{\text{path}} = \left(\frac{4\pi f d}{c}\right)^2 \tag{16}$$

where P_t is the transmit power, G_t and G_r are the antenna gains, f is the carrier frequency, d is the total path distance, c is the speed of light, and N_0 is the noise power. This channel model allows accurate evaluation of beamforming, phase tuning, and RIS placement strategies. Several studies [49–52] have validated the applicability of the Rician model in such systems, particularly in urban or elevated scenarios where LOS paths dominate. Once 100% LOS coverage is achieved, RIS phase shift optimization is carried out to maximize the system sum rate using various metaheuristic algorithms including Particle Swamp Optimization (PSO) [53], Grey Wolf Optimization (GWO) [54], Genetic Algorithm (GA) [55], Salp Swarm Algorithm (SSA) [56], and a hybrid PSO-GWO algorithm [57].

Algorithm 2 SA for RIS Placement Optimization

Input: Candidate positions *candPos*, building IDs *candBld*, user data, UAV position, buildings *blds*, number of RIS *numRIS*
Output: Optimized RIS positions *RISpos_SA*, coverage history *covSAhist*
Initialize: $T_0 \leftarrow 1.0$, $\alpha \leftarrow 0.995$, $maxIter \leftarrow 500$
$currSA \leftarrow$ random selection of *numRIS* candidates
$bestSA \leftarrow currSA$, $bestCovSA \leftarrow$ baseline UAV-only coverage
$covSAhist \leftarrow [bestCovSA]$
for $it = 1$ to $maxIter$ **do**
    $T \leftarrow T_0 \cdot \alpha^{(it-1)}$
    $nxt \leftarrow currSA$ with one random RIS index changed
    if any duplicates in nxt **then**
        continue
    end if
    $mask \leftarrow$ initial UAV coverage mask
    for each uncovered user k **do**
        for each RIS r in nxt **do**
            $p_{RIS} \leftarrow candPos[r]$
            $b_{RIS} \leftarrow candBld[r]$
            if LOS blocked from UAV to RIS or RIS to user k **then**
                continue
            else
                mark user k as covered; **break**
            end if
        end for
    end for
    $covNew \leftarrow$ fraction of users covered
    if $covNew > bestCovSA$ **or** rand() $< \exp\left(\frac{covNew - bestCovSA}{T}\right)$ **then**
        $currSA \leftarrow nxt$
        $bestSA \leftarrow currSA$
        $bestCovSA \leftarrow covNew$
    end if
    Append $bestCovSA$ to $covSAhist$
    if $bestCovSA \geq 1$ **then**
        break
    end if
end for
$RISpos\_SA \leftarrow candPos[bestSA]$

3.2.4. Sum Rate Maximization Problem Formulation

In RIS-assisted UAV communication systems, optimizing the phase shifts of RIS elements is critical to enhancing spectral efficiency and achieving robust coverage in complex

propagation environments. The RIS contributes additional signal paths by reflecting the incident signal from the UAV toward the users, and each element introduces a controllable phase shift to align the reflected wavefronts. The goal is to maximize the system-wide sum rate by jointly tuning these phase shifts, considering both the direct UAV-user link and RIS-assisted paths. The optimization problem can be formulated as shown in Equation (17),

$$\max_{\{\phi_{r,e}\}} \sum_{k=1}^{K} \log_2 \left(1 + \frac{P_t G_t G_r}{N_0} \left| h_{d,k} + \sum_{r=1}^{R} \sum_{e=1}^{N} G_{\text{RIS}} h_{ur}^{(r,e)} e^{j\phi_{r,e}} h_{rg}^{(r,e,k)} \right|^2 \right), \tag{17}$$

subject to the constraints in Equation (18),

$$\phi_{r,e} \in [0, 2\pi), \quad \forall r = 1, \ldots, R, \; e = 1, \ldots, N. \tag{18}$$

Here, $h_{d,k}$ denotes the direct LOS channel between the UAV and user k, while $h_{ur}^{(r,e)}$ and $h_{rg}^{(r,e,k)}$ represent the channels from the UAV to RIS element e on RIS r, and from the RIS element to user k, respectively. The reflected link is scaled by the RIS gain G_{RIS}, and $\phi_{r,e}$ is the tunable phase shift applied by the RIS element. This problem is non-convex due to the modulus square of a complex-valued sum and the coupling between variables, making traditional convex solvers ineffective. Metaheuristic optimization techniques are well suited to this type of problem, as they can efficiently search high-dimensional, non-convex spaces without requiring gradient information. Moreover, this formulation inherently supports blockage modeling by nullifying direct or reflected channel terms when the LOS path is obstructed, making it applicable in realistic urban or terrain-aware UAV-RIS deployment scenarios. The optimization objective is expressed in Equation (19),

$$R_{\text{sum}} = \sum_{k=1}^{K} \log_2 \left(1 + \frac{|\mathbf{h}_{\text{BU},k} + \mathbf{h}_{\text{RU},k}^H \boldsymbol{\Theta} \mathbf{h}_{\text{BR}}|^2}{\sigma^2} \right) \tag{19}$$

where $\boldsymbol{\Theta} = \text{diag}(e^{j\theta_1}, \ldots, e^{j\theta_N})$ is the RIS phase shift matrix. The hybrid PSO-GWO algorithm leverages the global search capability of PSO and the exploitation strength of GWO to improve convergence and solution accuracy. This integrated UAV-RIS system ensures full coverage and enhanced signal performance, representing a scalable and intelligent approach for 6G non-terrestrial networks (NTNs) [58–60].

In this setup, a UAV communicates with multiple ground users through both direct and RIS-assisted links. The communication channels are modeled using Rician fading, which captures the deterministic LOS component and the scattered NLOS component, making it suitable for UAV-based scenarios with elevated platforms and partial obstruction. The effective channel gain for the direct UAV-user link is expressed in Equation (20),

$$h_d = h_{\text{LOS}} \cdot \frac{\sqrt{PL_0}}{d_0} \cdot e^{-j\frac{2\pi d_0}{\lambda}}, \tag{20}$$

and

$$PL_0 = \left(\frac{\lambda}{4\pi} \right)^2 \tag{21}$$

where d_0 is the distance between the UAV and the user, λ is the carrier wavelength, and PL_0 is the free-space path loss at 1 m as expressed in Equation (21). Each RIS consists of N reflecting elements and the RIS-assisted signal component for user k is modeled as shown in Equation (22),

$$h_r = \sum_{r=1}^{R} \sum_{e=1}^{N} G_{\text{RIS}} \cdot h_{UR}^{(e)} \cdot e^{j\phi_e} \cdot h_{RU}^{(e)}, \tag{22}$$

where $h_{UR}^{(e)}$ and $h_{RU}^{(e)}$ represent the UAV-to-RIS and RIS-to-user channels for the e-th RIS element, respectively, G_{RIS} is the RIS gain, and ϕ_e is the optimized phase shift. In the case of active RIS, an additional gain term is included. The received SINR at user k is computed as shown in Equation (23),

$$\text{SINR}_k = \frac{P_t G_t G_r \cdot |h_d + h_r|^2}{N_0}, \tag{23}$$

where P_t is the UAV transmit power, G_t and G_r are the antenna gains, and N_0 is the noise power [61]. The total system throughput is then calculated as the sum-rate, which is expressed in Equation (24). The phase vector $\boldsymbol{\phi} \in [0, 2\pi]^{R \cdot N}$ is optimized to maximize R_{total} using metaheuristic algorithms.

$$R_{\text{total}} = \sum_{k=1}^{K} \log_2(1 + \text{SINR}_k). \tag{24}$$

3.3. Metaheuristic Algorithms

Metaheuristic algorithms represent a set of techniques aimed at solving problems, enabling the discovery of effective solutions that may not be the best, especially for intricate optimization challenges where conventional approaches falter. The main features of metaheuristic algorithms include population-based, stochastic, heuristic-driven, balanced exploration and exploitation capabilities, and problem independence. To optimize the phase shift in RIS-assisted UAV networks, we employ PSO, GWO, SSA, MPA, GA, and a hybrid PSO-GWO approach for comparative analysis. Table 1 shows the key features, advantages, and disadvantages of the algorithms used [53–57,62–65]. A hybrid PSO-GWO approach is also applied, where PSO is run for the first half of the iterations, and the best solution is used to seed GWO in the second half. This hybridization improves convergence behavior and overall sum-rate performance in the presence of Rician fading and multi-user interference [66,67].

Table 1. Comparison of metaheuristic algorithms.

Algorithm	Features	Advantages	Disadvantages
PSO	Swarm-based population Velocity and position updates	Simple, scalable and flexible Few control parameters	Trap to local optima for complex problems, sensitive to parameters
GWO	Wolf leadership hierarchy Encircling and hunting models	Balanced global and local search Robust for complex landscapes	Slower in high dimensions Sensitive to population size
SSA	Bio-inspired Salp swarm Leader and follower models	Fast convergence, flexible Few parameters, good exploration	Slow,trap to local optima Limited constraint handling
GA	Selection, crossover, mutation Genetics, probabilistic search	Flexible, global search, adaptable Handles discrete and continuous	Many parameters, slow Stochastic results, time-consuming
MPA	Marine predators, elite matrix Lévy and Brownian foraging	Strong exploration and exploitation Fast, robust for complex problems	Premature convergence diversity loss, computational cost
PSO–GWO	Exploits PSO's swarm intelligence with GWO's hierarchical strategy	Adaptable, fast convergence Robust for complex landscapes	More complex; tuning needed Potential redundancy

The various metaheuristic algorithms exhibit time and space complexities. PSO, GWO, MPA, and SSA have the same time complexities of $\mathcal{O}(N \times I \times D)$, and that of GA and hybrid PSO-GWO are $\mathcal{O}(N \times I \times D + N \log N)$ due to selection, sorting and $\mathcal{O}(N \times I \times D) + OH$ due to extra overhead (OH) for hybridization respectively. The space complexity is $\mathcal{O}(N \times D)$ for PSO, GWO, SSA, MPA, and hybrid PSO-GWO, and for GA, it

is $\mathcal{O}(N \times D + N)$, where N is the population size, I is number of iterations and D represents dimension of solution space [68–70].

3.4. Experimental Setup

We used MATLAB 2024a and the MATLAB toolbox running on a PC having 12th Gen Intel(R) Core(TM) i7-1270P 2.20 GHz, 16.0 GB RAM, a 64-bit operating system, an x64-based processor, and Windows 11 Pro for the experimental analysis and execution of the algorithms defined.

4. Results and Discussion

4.1. Link Budget Calculation and Outcomes

We first calculate the link budget for GES-LEO-UAV and BS-UAV as a dual backhaul link for reliable communication systems, working even if either of the links fails. First, we calculate the link budget for the base station (BS) and the UAV using the Equations (1) and (2), considering the nearly realistic values and assumptions described in Section 3.1.1. The calculated path loss is within the range detectable by the receiver to ensure QoS. Table 2 shows the parameters for the BS-UAV link budget.

Table 2. Parameters used in BS-to-UAV link budget calculation at 28 GHz.

Parameter	Value	Unit
Transmit Power (P_t)	30	dBm
Transmit Antenna Gain (G_t)	15	dBi
Receiver Antenna Gain (G_r)	5	dBi
Carrier Frequency (f)	28	GHz
Propagation Distance (d)	1000	m
Free Space Path Loss (L_p)	121.39	dB
Miscellaneous Losses (L_m)	3	dB
Speed of Light (c)	3×10^8	m/s
Received Power (P_r)	–74.39	dBm

Then we calculated the link budget for the satellite earth station to UAV, through LEO, to have a backhaul as a redundant link for service reliability. We employed a free-space path propagation model for path loss and assumed realistic values for other parameters and used Equations (2)–(6), as illustrated in Section 3.1.2. Table 3 shows the parameters used for the link budget calculation for GES to LEO satellite and their outcomes.

4.2. UAV and RIS Placement Optimization

We simulate a communication environment supported by a UAV within a 300 m × 300 m urban area, where a UAV is deployed in the center of the region at an altitude of 100 m. A total of 72 ground users (22 are discarded as they are within building footprints) are randomly distributed across the area, each positioned at a height of 1.5 m. The environment includes six rectangular buildings that may obstruct line-of-sight (LOS) paths between the UAV and users. These buildings have fixed heights of 50 m and are defined by their 2D footprints: B1 spans (20–270 m, 220–270 m), B2 spans (200–220 m, 20–130 m), B3 spans (20–100 m, 50–70 m), B4 spans (100–120 m, 70–200 m), B5 spans (150–270 m, 130–150 m), and B6 spans (10–100 m, 180–200 m). Users located within any building footprint are excluded from the simulation. For each remaining user, we evaluate whether the direct UAV-to-user link is obstructed by any building using geometric intersection, detection and 3D ray height comparison. Users are then classified as either having LOS or being blocked, based on whether the ray intersects a building below its roofline. The result shows that 62% of users are LOS with UAVs and the remaining 38% have NLOS with UAVs.

Table 3. Link budget calculation for LEO-ground satellite communication.

Parameter	Value	Unit
Input Parameters		
Carrier frequency (f)	28	GHz
Distance to satellite (d)	500	km
Transmit power (P_t)	43	dBm
Transmit antenna gain (G_t)	30	dBi
Receive antenna gain (G_r)	30	dBi
Transmitter losses (L_{tx})	2	dB
Receiver losses (L_{rx})	2	dB
Atmospheric losses (L_{atm})	2	dB
Bandwidth (B)	100	MHz
Noise temperature (T)	500	K
Boltzmann constant (k)	1.38×10^{-23}	J/K
Calculated Outcomes		
Free space path loss (L_{FSPL})	175.37	dB
Received power (P_r)	−78.37	dBm
Noise power (N)	−91.61	dBm
Carrier-to-noise ratio ($\frac{C}{N}$)	13.24	dB

Figure 2a,b show the 2D and 3D layout of the initial deployment of UAVs, obstacles, and users. The connection between UAV and user with green and red lines shows the LOS and NLOS, respectively. To improve the LOS between UAV and user or coverage footprint, we optimize the position of the UAV by moving the XY plane, thus maintaining a constant height of 100m by a grid search algorithm with a grid size of 10 m, since there is a single UAV. The objective is to increase LOS users as in Equation (8) subject to the constraint of Equation (9). The coverage is increased to 68% after grid search as detailed in Algorithm 1. Figure 2c shows the coverage heat map of grid search, and Figure 2d shows coverage in each iteration. Figure 2e,f show the 2D and 3D deployment after the grid search algorithm, showing the coverage improvement.

To improve the coverage further, i.e, full coverage, we introduce RIS one by one, starting with a single RIS to minimize resources and optimize the location of RIS. Then we add one RIS each time till 100% coverage (ubiquitous connectivity) is achieved. Adding a RIS initially improves coverage to 96%. SA is used for optimization as described in Algorithm 2. Figure 3a shows the coverage against each iteration with a single RIS. Then we add RIS each time iteratively and use SA optimization, and we obtain full coverage with two RIS. Figure 3b shows the coverage convergence, achieving 100% with 2 RISs. Figure 3c,d show the optimized placement of UAV-RIS using SA, ensuring LOS from UAV or RIS to all users.

4.3. RIS Phase Shift Optimization Under Rician Fading

After achieving LOS of all users (100% coverage), we build a set where a UAV communicates with multiple ground users through both direct and RIS-assisted links. Table 4 shows the parameters used for UAV-RIS-users access networks.

We calculate the effective channel gain of the UAV to the user's direct signal using Rician fading using Equation (20) with free space reference path loss at 1 m using Equation (21). We consider the number of elements of an RIS to be 64, and we model the RIS-assisted signal between the UAV and a user using Equation (22). Then we calculate SINR at any user using Equation (23). The total sum rate is calculated using Equation (24). The sum rate is 9.8593 bits/s/Hz for the initial deployment of UAV and 10.7762 bits/s/Hz after placement optimization of UAV due to the increase in LOS users.

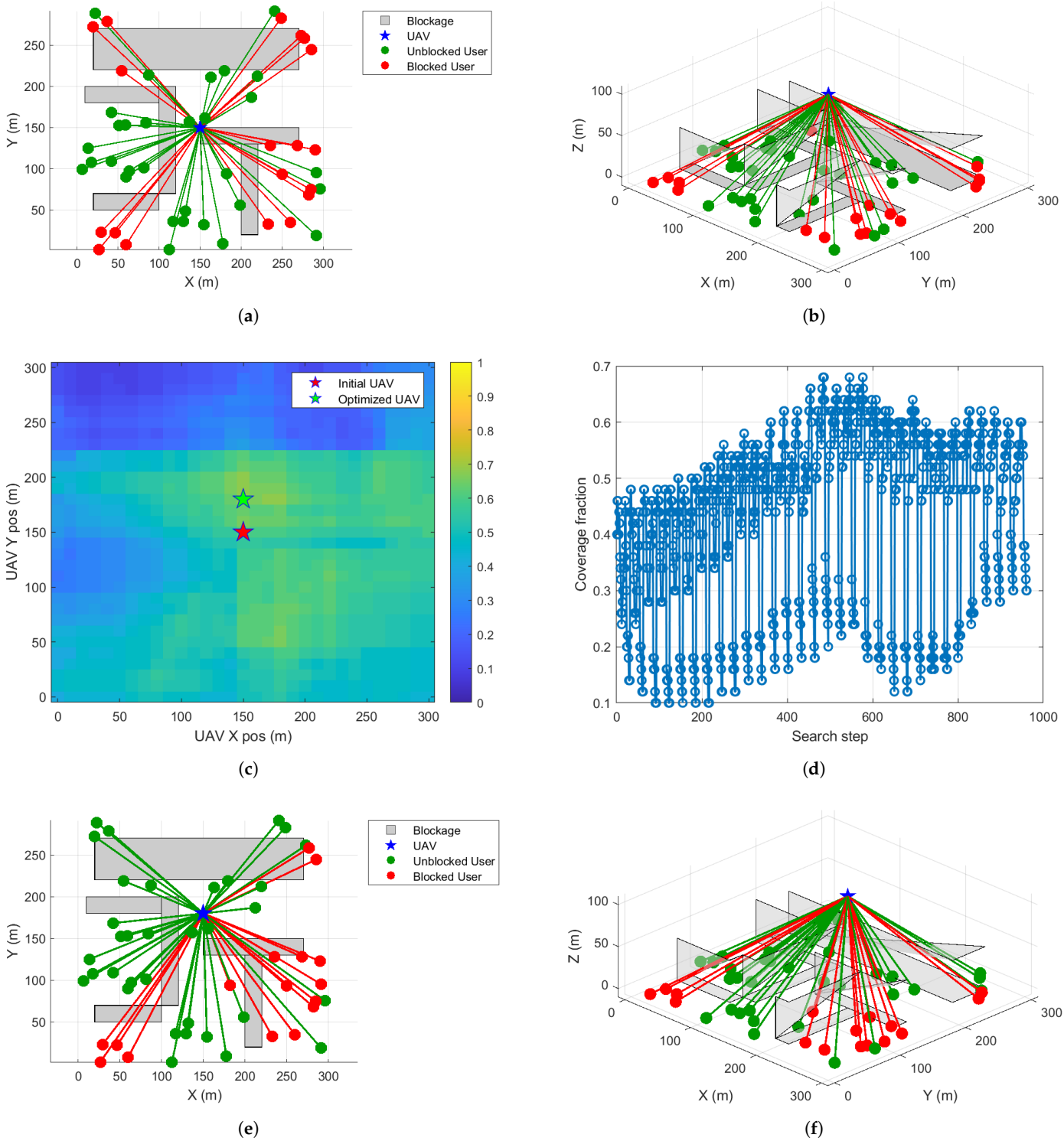

Figure 2. Initial deployment: (**a**) 2D schematic; (**b**) 3D schematic. UAV optimized deployment: (**c**) coverage heatmap; (**d**) coverage vs. iteration; (**e**) optimized 2D schematic; (**f**) optimized 3D schematic.

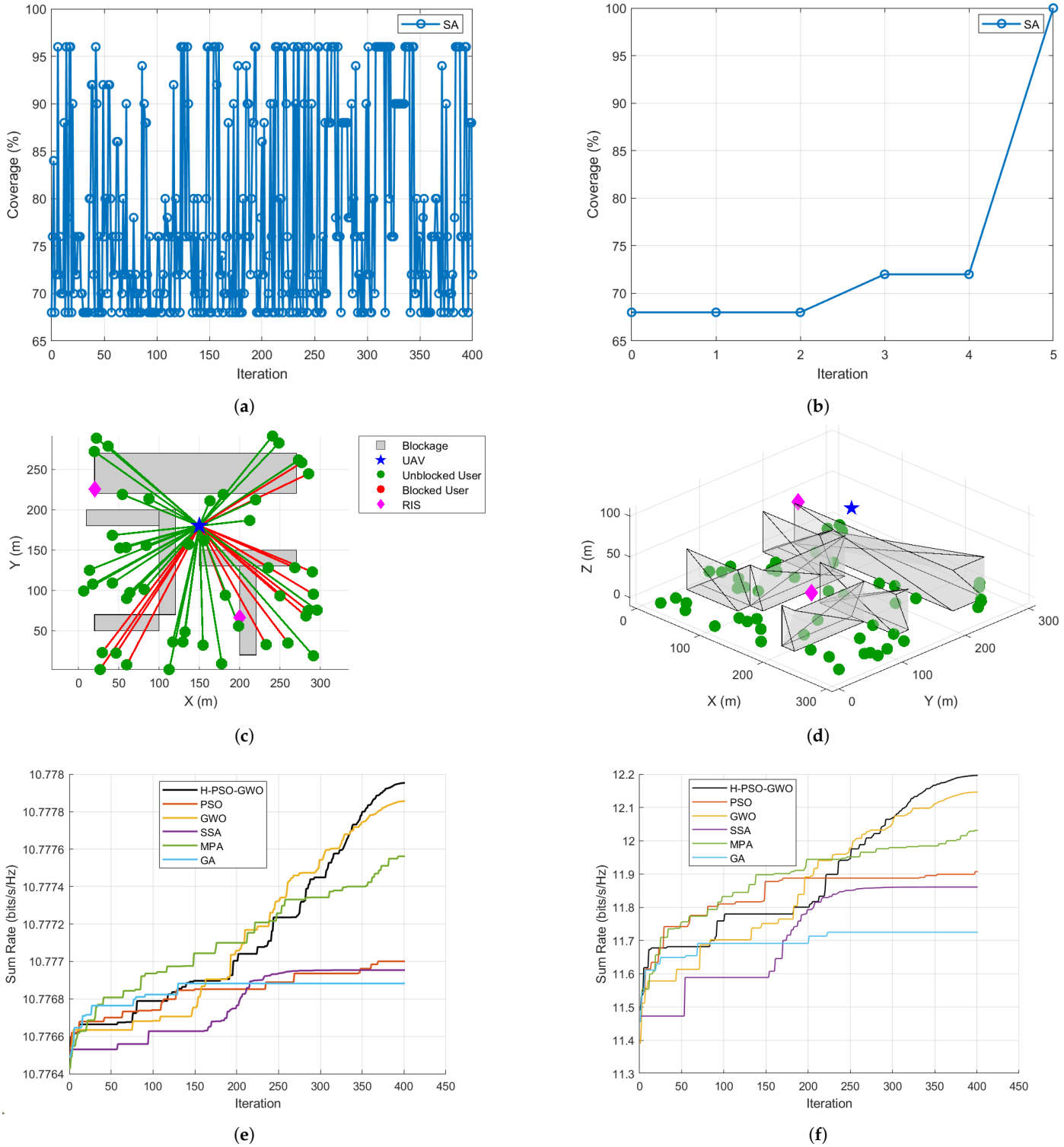

Figure 3. SA optimization for RIS placement: (**a**) coverage vs. iterations with 1 RIS; (**b**) coverage convergence with 2 RISs; (**c**) 2D schematic; (**d**) 3D schematic. Sum rate by phase shift optimization: (**e**) passive RIS; (**f**) active RIS.

Table 4. UAV-RIS-users access network input parameters.

Parameter	Value	Unit
Carrier Frequency (f_0)	28	GHz
Wavelength ($\lambda = c/f_0$)	0.0107	m
UAV Transmit Power (P_t)	43	dBm
UAV Antenna Gain (G_t)	20	dBi
User Antenna Gain (g_r)	0	dBi
RIS Tile Gain (Passive) (G_{RIS})	0	dBi
RIS Tile Gain (Active) ($A_{G_{\text{RIS}}}$)	20	dBi
Receiver Noise Floor (N_0)	-90	dBm
Rician K-factor (K)	10	dB
Number of RIS elements (N_{elem})	64	–
Scatter variance (σ)	1	–
RIS element spacing (d_{elem})	$\lambda/2$	m

We used metaheuristic algorithms PSO, GWO, SSA, MPA, GA, and hybrid PSO-GWO to evaluate the comparative performance of phase shift optimization. Table 5 shows the initial parameters used for phase shift optimization to have maximum average sum rate.

Table 5. Metaheuristic algorithm parameters used in UAV-RIS optimization.

Parameters	Values
GA	Tournament selection; single-point crossover; mutation rate 0.1 per generation
PSO	Inertia w = 0.7, cognitive/social factors $c_1 = c_2 = 1.5$
GWO	Convergence coefficient a linearly decreases from 2 to 0
SSA	Salp leader coefficient $c_1 = 2\exp\left(-(4t/T)^2\right)$, chain update for followers
MPA	Predator—prey switch probability $(0.1 + t\,(0.8/T))$, Lévy exponent $\beta = 1.5$

Figure 3e,f show each algorithm's average sum rate convergence of passive and active RIS, respectively. In both cases, hybrid PSO-GWO shows the best average sum rate. Figure 4a shows the sum rate outcome after phase shift optimization for active and passive RIS, and the best value of sum rate is 10.778 bits/s/Hz for passive RIS from hybrid PSO-GWO. The average sum rate is not improved due to a dominant direct UAV-users signal, as passive RIS does not amplify the signal. We then optimized for active RIS with a gain of 20 dBi, resulting in the improvement of the sum rate of active RIS over passive RIS, and the best value of sum rate is 12.1962 bits/s/Hz from hybrid PSO-GWO. Figure 4b shows the phase element index heatmap against each iteration. Since the sum rate increment depends on the transmit power, the number of RIS elements, and the gain of active RIS, we analyzed the impact of these parameters by varying the values of particular parameters, maintaining the constant values of other parameters. Figure 4c shows the sum rate outcomes against the different transmitted power values. The result indicates that the sum rate can be increased significantly if we increase the transmit power. Similarly, Figure 4d,e show that the sum rate can also be increased by increasing the gain of active RIS and the number of RIS elements, respectively. The comparative values show that the gain of active RIS significantly impacts the average sum rate of the users. Figure 4f shows the sum rate variation with the number of users.

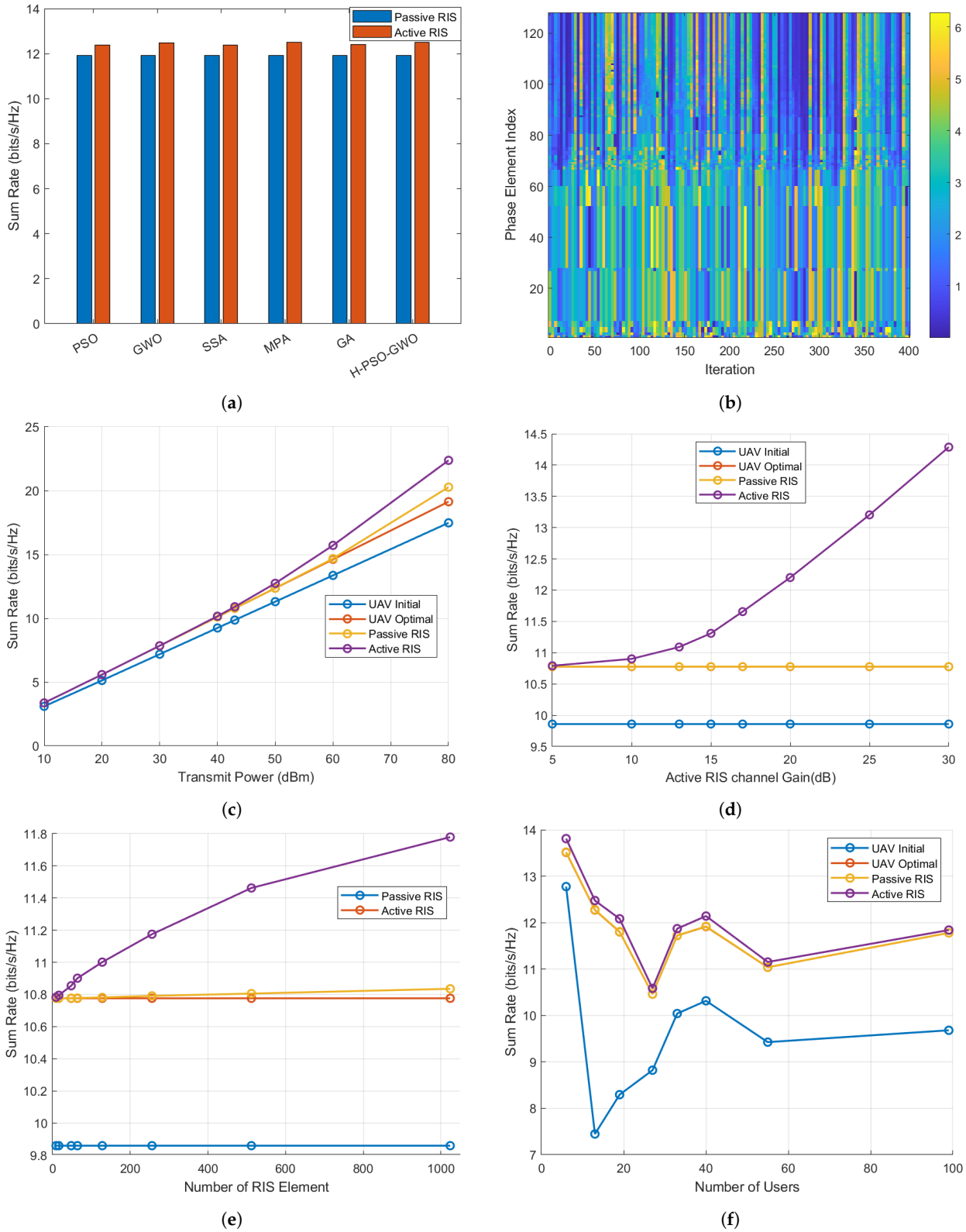

Figure 4. Sum rate by phase shift optimization: (**a**) comparative bar chart; (**b**) heatmap of hybrid PSO-GWO). Sum rate variation: (**c**) sum rate vs. transmit power; (**d**) sum rate vs. active RIS gain; (**e**) sum rate vs. number of RIS reflecting elements; (**f**) sum rate vs. number of users.

The UAV placement using a grid search algorithm, incremental deployment of RIS, and phase shift optimization using metaheuristic algorithms to maximize the sum rate one after another results in a joint increase in coverage and spectrum efficiency. The results

show that spectrum efficiency increased by 9.299% and coverage by 6% after UAV placement using the grid search algorithm. Then, the deployment of passive RIS results in a 32% increase in LOS users, along with a 9.31% increase in spectrum efficiency. The coverage improved significantly with the passive RIS, but the spectrum efficiency was not significantly enhanced, i.e., by 0.011% (from 9.299% to 9.31%) only. The replacement of active RIS with passive RIS results in an increase in spectrum efficiency of up to 12.1962 bits/s/Hz, representing a 23.7% improvement compared to the spectrum efficiency before placement and phase shift optimization. Figure 5a shows the average fitness values, and Figure 5b shows the variance fitness values, indicating that the higher average sum rate values and lower variance values for hybrid PSO-GWO show that hybrid PSO-GWO outperforms other metaheuristic algorithms used.

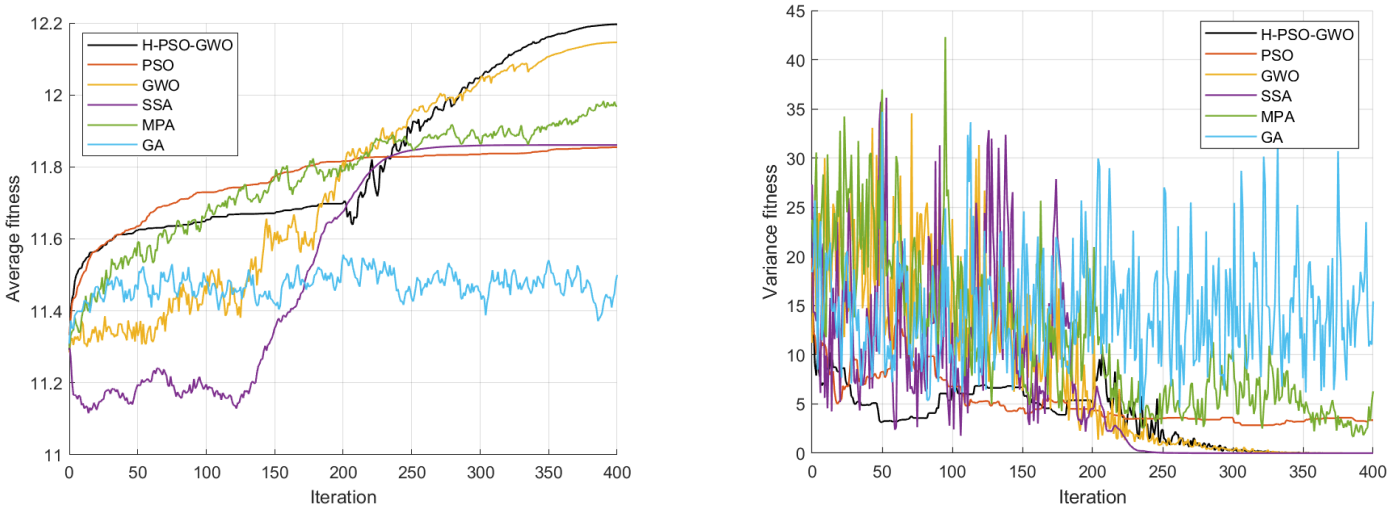

(**a**) (**b**)

Figure 5. Comparative values: (**a**) average fitness; (**b**) variance fitness.

5. Conclusions and Future Directions

In this study, we presented an integrated UAV-LEO-RIS communication framework with dual wireless backhaul designed to enhance data throughput and coverage in next-generation wireless networks. The framework strategically combines UAVs, LEO satellites, and RIS to optimize network performance. We employed a grid search method for UAV placement optimization, SA for RIS deployment, and PSO, GWO, SSA, GA, MPA, and a hybrid PSO-GWO for sum rate maximization. Simulation results demonstrate that the hybrid PSO-GWO algorithm outperforms individual metaheuristics in terms of convergence speed and achieving higher sum rates, offering a robust solution for scenarios requiring rapid deployment and high data throughput. The sum rate can be significantly increased from 9.8593 bits/s/Hz to 10.7762 bits/s/Hz and the LOS rate from 62% to 68% using the Grid search algorithm. SA optimization results in further improvement in LOS coverage from 68% to 100%, adding two RISs. Although increasing the transmit power greatly enhances the sum rate, practical power constraints at the transmitter make it impossible to increase it indefinitely. The sum rate is increased significantly with the increase in active RIS gain. This active component can be installed on top of building walls, and it plays an important role in having 100% LOS coverage and increasing the spectrum efficiency from 9.8593 bits/s/Hz to 12.1962 bits/s/Hz, i.e., 23.7%. This plays a crucial role in achieving ubiquitous coverage and improved spectrum efficiency.

Future efforts will include modeling users with mobility, dynamic obstacles, and real-world case studies. To further enhance the capabilities of the proposed framework, future

research can explore multiple UAV-RIS-assisted network optimization; the incorporation of deep reinforcement learning, energy efficiency optimization, scalability, and real-world deployment; and integration with Emerging Technologies such as NOMA, MEC, and intelligent scheduling frameworks.

Author Contributions: Conceptualization, N.R.K., B.R.D. and S.R.J.; methodology, N.R.K. and B.R.D.; software, N.R.K.; validation, N.R.K., B.R.D. and S.R.J.; formal analysis, N.R.K.; investigation, B.R.D. and S.R.J.; resources, B.R.D.; data curation, N.R.K.; writing—original draft preparation, N.R.K.; writing—review and editing, N.R.K., B.R.D. and S.R.J.; visualization, N.R.K.; supervision, B.R.D. and S.R.J.; project administration, B.R.D.; funding acquisition, B.R.D. All authors have read and agreed to the published version of the manuscript.

Funding: This research was supported by University Grants Commission, Nepal (Grants ID: CRG-078/79-Engg-01) principally investigated by Dr. Babu R. Dawadi.

Institutional Review Board Statement: Not applicable.

Informed Consent Statement: Not applicable.

Data Availability Statement: The raw data supporting the conclusions of this article will be made available by the authors on request.

Acknowledgments: The language correction AI tools such as Grammarly and Quillbot were used for this manuscript to ensure that the sentences were grammatically correct and to improve English sentence structure for clarity. After using these tools, the authors reviewed and edited the content as needed and take full responsibility for the content of the publication. We are thankful to reviewers for their constructive comments.

Conflicts of Interest: The authors declare no conflicts of interest.

References

1. Pogaku, A.C.; Do, D.T.; Lee, B.M.; Nguyen, N.D. UAV-assisted RIS for future wireless communications: A survey on optimization and performance analysis. *IEEE Access* **2022**, *10*, 16320–16336. [CrossRef]
2. Khatiwoda, N.R.; Dawadi, B.R.; Joshi, S.R. An Integrated Architecture of RIS-based Non-Terrestrial Networks with 6G for Rural Communications. In Proceedings of the 2024 International Conference on Emerging Technologies and Innovation for Sustainability (EmergIN), Greater Noida, India, 20–21 December 2024; pp. 30–36.
3. Khatiwoda, N.R.; Dawadi, B.R.; Joshi, S.R. Capacity and Coverage Dimensioning for 5G Standalone Mixed-Cell Architecture: An Impact of Using Existing 4G Infrastructure. *Future Internet* **2024**, *16*, 423. [CrossRef]
4. Khaled, A.; Alwakeel, A.S.; Shaheen, A.M.; Fouda, M.M.; Ismail, M.I. Placement optimization and power management in a multiuser wireless communication system with reconfigurable intelligent surfaces. *IEEE Open J. Commun. Soc.* **2024**, *5*, 4186–4206. [CrossRef]
5. Xu, Q.; You, Q.; Gong, Y.; Yang, X.; Wang, L. RIS-assisted UAV-enabled green communications for industrial IoT exploiting deep learning. *IEEE Internet Things J.* **2024**, *11*, 26595–26609. [CrossRef]
6. Toka, M.; Lee, B.; Seong, J.; Kaushik, A.; Lee, J.; Lee, J.; Lee, N.; Shin, W.; Poor, H.V. RIS-empowered LEO satellite networks for 6G: Promising usage scenarios and future directions. *IEEE Commun. Mag.* **2024**, *11*, 128–135. [CrossRef]
7. Shayea, I.; El-Saleh, A.A.; Ergen, M.; Saoud, B.; Hartani, R.; Turan, D.; Kabbani, A. Integration of 5G, 6G and IoT with Low Earth Orbit (LEO) networks: Opportunity, challenges and future trends. *Results Eng.* **2024**, *23*, 102409. [CrossRef]
8. Mohamed, E.M.; Rihan, M. Bandit approach for unmanned aerial vehicle-centric low earth orbit satellite selection. *Digit. Signal Process.* **2024**, *151*, 104546. [CrossRef]
9. Zhou, L.; Xu, W.; Wang, C.; Chen, H.H. Ris-enabled uav cognitive radio networks: Trajectory design and resource allocation. *Information* **2023**, *14*, 75. [CrossRef]
10. Othman, W.M.; Ateya, A.A.; Nasr, M.E.; Muthanna, A.; ElAffendi, M.; Koucheryavy, A.; Hamdi, A.A. Key Enabling Technologies for 6G: The Role of UAVs, Terahertz Communication, and Intelligent Reconfigurable Surfaces in Shaping the Future of Wireless Networks. *J. Sens. Actuator Netw.* **2025**, *14*, 30. [CrossRef]
11. Worka, C.E.; Khan, F.A.; Ahmed, Q.Z.; Sureephong, P.; Alade, T. Reconfigurable Intelligent Surface (RIS)-Assisted Non-Terrestrial Network (NTN)-Based 6G Communications: A Contemporary Survey. *Sensors* **2024**, *24*, 6958. [CrossRef]

12. Ma, T.; Zhou, H.; Qian, B.; Cheng, N.; Shen, X.; Chen, X.; Bai, B. UAV-LEO integrated backbone: A ubiquitous data collection approach for B5G internet of remote things networks. *IEEE J. Sel. Areas Commun.* **2021**, *39*, 3491–3505. [CrossRef]
13. Chen, R.; Wang, W.; Wu, W. An Adjustable Wireless Backhaul Link Selection Algorithm for LEO-UAV-Sensor-Based Internet of Remote Things Network. *Sensors* **2024**, *24*, 1973. [CrossRef]
14. Janji, S.; Wawrzyniak, P.; Formanowicz, P.; Kliks, A. Integrating UAV-Enabled Base Stations in 3D Networks: QoS-Aware Joint Fronthaul and Backhaul Design. *arXiv* **2024**, arXiv:2404.17547.
15. Yu, B.; Zhang, J.; Chen, J.; Xu, Y.; Gao, R.; Wang, J. Aerial RIS-Enabled Wireless Coverage Enhancement Under UAV Jitter. In Proceedings of the 2023 IEEE 23rd International Conference on Communication Technology (ICCT), Wuxi, China, 20–22 October 2023; pp. 1716–1721.
16. El Hammouti, H.; Saoud, A.; Ennahkami, A.; Bergou, E.H. Energy Efficient Aerial RIS: Phase Shift Optimization and Trajectory Design. In Proceedings of the 2024 IEEE 99th Vehicular Technology Conference (VTC2024-Spring), Singapore, 24–27 June 2024; pp. 1–7.
17. Wei, Z.; Cai, Y.; Sun, Z.; Ng, D.W.K.; Yuan, J.; Zhou, M.; Sun, L. Sum-rate maximization for IRS-assisted UAV OFDMA communication systems. *IEEE Trans. Wirel. Commun.* **2020**, *20*, 2530–2550. [CrossRef]
18. Jia, H.; Chen, G.; Huang, C.; Dang, S.; Chambers, J.A. Trajectory and phase shift optimization for RIS-equipped UAV in FSO communications with atmospheric and pointing error loss. *Electronics* **2023**, *12*, 4275. [CrossRef]
19. Elnabty, I.A.; Fahmy, Y.; Kafafy, M. A survey on UAV placement optimization for UAV-assisted communication in 5G and beyond networks. *Phys. Commun.* **2022**, *51*, 101564. [CrossRef]
20. Darem, A.A.; Alkhaldi, T.M.; Alhashmi, A.A.; Mansouri, W.; Alghawli, A.S.A.; Al-Hadhrami, T. Optimizing resource allocation for enhanced urban connectivity in LEO-UAV-RIS networks. *J. King Saud Univ.—Comput. Inf. Sci.* **2024**, *36*, 102238. [CrossRef]
21. Yao, Y.; Lv, K.; Huang, S.; Li, X.; Xiang, W. UAV trajectory and energy efficiency optimization in RIS-assisted multi-user air-to-ground communications networks. *Drones* **2023**, *7*, 272. [CrossRef]
22. Huroon, A.M.; Huang, Y.C.; Wang, L.C. Optimized transmission strategy for UAV-RIS 2.0 assisted communications using rate splitting multiple access. In Proceedings of the 2023 IEEE 98th Vehicular Technology Conference (VTC2023-Fall), Hong Kong, China, 10–13 October 2023; pp. 1–6.
23. Zeng, S.; Zhang, H.; Di, B.; Han, Z.; Song, L. Reconfigurable intelligent surface (RIS) assisted wireless coverage extension: RIS orientation and location optimization. *IEEE Commun. Lett.* **2020**, *25*, 269–273. [CrossRef]
24. Tran, T.T.M.; Vu, B.M.; Shin, O.S. Optimization of Bandwidth Allocation and UAV Placement in Active RIS-Assisted UAV Communication Networks with Wireless Backhaul. *Drones* **2025**, *9*, 111. [CrossRef]
25. Zhang, Q.; Zhao, J.; Zhang, R.; Yang, L. Downlink Transmissions of UAV-RIS-Assisted Cell-Free Massive MIMO Systems: Location and Trajectory Optimization. *Sensors* **2024**, *24*, 4064. [CrossRef]
26. Jeon, H.B.; Park, S.H.; Park, J.; Huang, K.; Chae, C.B. An energy-efficient aerial backhaul system with reconfigurable intelligent surface. *IEEE Trans. Wirel. Commun.* **2022**, *21*, 6478–6494. [CrossRef]
27. Zhang, W.; Li, J.; Yu, W.; Ding, P.; Wang, J.; Zhang, X. Algorithm for UAV path planning in high obstacle density environments: RFA-star. *Front. Plant Sci.* **2024**, *15*, 1391628. [CrossRef] [PubMed]
28. Ahmed, M.; Soofi, A.A.; Khan, F.; Raza, S.; Khan, W.U.; Su, L.; Xu, F.; Han, Z. Toward a Sustainable Low-Altitude Economy: A Survey of Energy-Efficient RIS-UAV Networks. *arXiv* **2025**, arXiv:2504.02162.
29. Mihertie, H.D.; Wang, Z. Resource allocation for UAV-RIS-assisted RSMA system with hardware impairments. *Comput. Netw.* **2025**, *266*, 111336. [CrossRef]
30. Saleh, A.M.; Omar, S.S.; Abd El-Haleem, A.M.; Ibrahim, I.I.; Abdelhakam, M.M. Trajectory optimization of UAV-IRS assisted 6G THz network using deep reinforcement learning approach. *Sci. Rep.* **2024**, *14*, 18501. [CrossRef]
31. Maral, G.; Bousquet, M. *Satellite Communications Systems: Systems, Techniques and Technology*, 5th ed.; Wiley: Hoboken, NJ, USA, 2009.
32. Xiao, Z.; Xia, P.; Xia, X.G. Enabling UAV cellular with millimeter-wave communication: Potentials and approaches. *IEEE Commun. Mag.* **2016**, *54*, 66–73. [CrossRef]
33. Mozaffari, M.; Saad, W.; Bennis, M.; Debbah, M. A tutorial on UAVs for wireless networks: Applications, challenges, and open problems. *IEEE Commun. Surv. Tutor.* **2019**, *21*, 2334–2360. [CrossRef]
34. Alghamdi, R; Alhadrami, R; Alhothali, D; Almorad, H; Faisal, A; Helal, S; Shalabi, R; Asfour, R, Hammad, N; Shams, A; et al. Intelligent Surfaces for 6G Wireless Networks: A Survey of Optimization and Performance Analysis Techniques. *IEEE access.* **2020**, *8*, 202795–202818. [CrossRef]
35. ITU-R. Propagation Data and Prediction Methods Required for the Design of Earth-Space Telecommunication Systems. Recommendation ITU-R P.618-13. 2017. Available online: https://www.itu.int/rec/R-REC-P.618/en (accessed on 14 March 2025).
36. Giordani, M.; Polese, M.; Mezzavilla, M.; Rangan, S.; Zorzi, M. Toward 6G Networks: Use Cases and Technologies. *IEEE Commun. Mag.* **2020**, *58*, 55–61. [CrossRef]
37. Rappaport, T.S. *Wireless Communications: Principles and Practice*, 2nd ed.; Prentice Hall: Hoboken, NJ, USA, 2002.

38. Lin, M.; Huang, Q.; Cola, T.D.; Wang, J.B.; Wang, J.; Guizani, M.; Wang, J.Y. Integrated 5G-satellite networks: A perspective on physical layer reliability and security. *IEEE Wirel. Commun.* **2020**, *27*, 152–159. [CrossRef]
39. Saboor, A.; Vinogradov, E.; Cui, Z.; Pollin, S. Probability of line of sight evaluation in urban environments using 3D simulator. In Proceedings of the 2023 IEEE International Black Sea Conference on Communications and Networking (BlackSeaCom), Istanbul, Turkiye, 4–7 July 2023; pp. 135–140.
40. Dufour, J.M.; Neves, J. Finite-sample inference and nonstandard asymptotics with Monte Carlo tests and R. In *Handbook of Statistics*; Elsevier: Boca Raton, FL, USA, 2019; Volume 41, pp. 3–31.
41. Kang, Z.; You, C.; Zhang, R. Placement learning for multi-UAV relaying: A Gibbs sampling approach. In Proceedings of the ICC 2020—2020 IEEE International Conference on Communications (ICC), Dublin, Ireland, 7–11 June 2020; pp. 1–6.
42. Zhang, T.; Lei, J.; Liu, Y.; Feng, C.; Nallanathan, A. Trajectory optimization for UAV emergency communication with limited user equipment energy: A safe-DQN approach. *IEEE Trans. Green Commun. Netw.* **2021**, *5*, 1236–1247. [CrossRef]
43. Mazaherifar, A.; Mostafavi, S. UAV placement and trajectory design optimization: A survey. *Wirel. Pers. Commun.* **2022**, *124*, 2191–2210. [CrossRef]
44. Xu, Y.; Zhang, T; Liu, Y.; Yang, D.; Xiao, L.; Tao, M. Computation capacity enhancement by joint UAV and RIS design in IoT. *IEEE Internet Things J.* **2022**, *9*, 20590–20603. [CrossRef]
45. Tang, X; Xiong, Z; Dong, L; Zhang, R; Du, Q. UAV-enabled aerial active RIS with learning deployment for secured wireless communications. *Chin. J. Aeronaut.* **2024**, 103383. [CrossRef]
46. Kirkpatrick, S.; Gelatt, C.D.; Vecchi, M.P. Optimization by simulated annealing. *Science* **1983**, *220*, 671–680. [CrossRef]
47. Aarts, E.; Korst, J. *Simulated Annealing and Boltzmann Machines: A Stochastic Approach to Combinatorial Optimization and Neural Computing*; Wiley-Interscience: Hoboken, NJ, USA, 1989.
48. Zhai, L.; Zou, Y.; Zhu, J.; Jiang, Y. RIS-assisted UAV-enabled wireless powered communications: System modeling and optimization. *IEEE Trans. Wirel. Commun.* **2023**, *23*, 5094–5108. [CrossRef]
49. Basar, E.; Di Renzo, M.; De Rosny, J.; Debbah, M.; Alouini, M.S.; Zhang, R. Wireless communications through reconfigurable intelligent surfaces. *IEEE Access* **2019**, *7*, 116753–116773. [CrossRef]
50. Wu, Q.; Zhang, R. Towards smart and reconfigurable environment: Intelligent reflecting surface aided wireless network. *IEEE Commun. Mag.* **2020**, *58*, 106–112. [CrossRef]
51. Zeng, Y.; Zhang, R.; Lim, T.J. Wireless communications with unmanned aerial vehicles: Opportunities and challenges. *IEEE Commun. Mag.* **2016**, *54*, 36–42. [CrossRef]
52. Pan, C.; Ren, H.; Wang, K.; Elkashlan, M.; Nallanathan, A.; Wang, J.; Hanzo, L. Intelligent reflecting surface aided MIMO broadcasting for simultaneous wireless information and power transfer. *IEEE J. Sel. Areas Commun.* **2020**, *38*, 1719–1734. [CrossRef]
53. Kennedy, J.; Eberhart, R. Particle swarm optimization. In Proceedings of the ICNN'95—International Conference on Neural Networks, Perth, WA, Australia, 27 November–1 December 1995; Volume 4, pp. 1942–1948.
54. Mirjalili, S.; Mirjalili, S.M.; Lewis, A. Grey Wolf Optimizer. *Adv. Eng. Softw.* **2014**, *69*, 46–61. [CrossRef]
55. Holland, J.H. *Adaptation in Natural and Artificial Systems: An Introductory Analysis with Applications to Biology, Control, and Artificial Intelligence*; MIT Press: Cambridge, MA, USA, 1992.
56. Mirjalili, S.; Gandomi, A.H.; Mirjalili, S.Z.; Saremi, S.; Faris, H.; Mirjalili, H. Salp Swarm Algorithm: A bio-inspired optimizer for engineering design problems. *Adv. Eng. Softw.* **2017**, *114*, 163–191. [CrossRef]
57. Şenel, F.A.; Gökçe, F.; Yüksel, A.S.; Yiğit, T. A novel hybrid PSO–GWO algorithm for optimization problems. *Eng. Comput.* **2019**, *35*, 1359–1373. [CrossRef]
58. Wu, Q.; Zhang, R. Intelligent reflecting surface-aided wireless communications: A tutorial. *IEEE Trans. Commun.* **2021**, *69*, 3313–3351. [CrossRef]
59. Di Renzo, M.; Zappone, A.; Debbah, M.; Alouini, M.S.; Yuen, C.; De Rosny, J.; Tretyakov, S. Smart radio environments empowered by AI reconfigurable meta-surfaces: An overview. *IEEE J. Sel. Areas Commun.* **2020**, *38*, 2450–2525. [CrossRef]
60. Abuzgaia, N.; Younis, A.; Mesleh, R. UAV Communications in 6G Cell-Free Massive MIMO Systems. In Proceedings of the 2023 IEEE 3rd International Maghreb Meeting of the Conference on Sciences and Techniques of Automatic Control and Computer Engineering (MI-STA), Benghazi, Libya, 21–23 May 2023; pp. 634–639.
61. Zhang, J.; Björnson, E.; Matthaiou, M.; Ng, D.W.K.; Yang, H.; Love, D.J. Prospective multiple antenna technologies for beyond 5G. *IEEE J. Sel. Areas Commun.* **2020**, *38*, 1637–1660. [CrossRef]
62. Poli, R. Analysis of the publications on the applications of particle swarm optimization. *J. Artif. Evol. Appl.* **2008**, *2008*, 685175.
63. Castelli, M.; Manzoni, L.; Mariot, L.; Nobile, M. S.; Tangherloni, A. Salp swarm optimization: A critical review. *Expert Syst. Appl.* **2022**, *189*, 116029. [CrossRef]
64. Faramarzi, S.; Heidarinejad, M.; Gandomi, A.H. Marine Predators Algorithm: A Nature-Inspired Metaheuristic. *Expert Syst. Appl.* **2020**, *152*, 113377. [CrossRef]

65. Rai, R.; Dhal, K.G.; Das, A.; Ray, S. An inclusive survey on marine predators algorithm: Variants and applications. *Arch. Comput. Methods Eng.* **2023**, *30*, 3133–3172. [CrossRef]
66. Prasad, R.; Roy, A.; Kumari, S. Enhancing Cloud Task Scheduling Using a Hybrid Particle Swarm and Grey Wolf Optimization Approach. *arXiv* **2025**, arXiv:2505.15171. [CrossRef]
67. Houssein, E.H.; Saad, M.R.; Djenouri, Y.; Hu, G.; Ali, A.A.; Shaban, H. Metaheuristic algorithms and their applications in wireless sensor networks: review, open issues, and challenges. *Clust. Comput.* **2024**, *27*, 13643–13673. [CrossRef]
68. Yang, X.S. Nature-inspired optimization algorithms: Challenges and open problems. *J. Comput. Sci.* **2020**, *46*, 101104. [CrossRef]
69. Talbi, E.G. *Metaheuristics: From Design to Implementation*; Wiley: Hoboken, NJ, USA, 2009.
70. Huang, T.; Yin, H.; Huang, X. Improved genetic algorithm for multi-threshold optimization in digital pathology image segmentation. *Sci. Rep.* **2024**, *14*, 22454. [CrossRef]